Evaluation and optimization of lidar temperature analysis algorithms using simulated data.

Thierry Leblanc, I. Stuart McDermid
Jet Propulsion Laboratory, California Institute of Technology, Table Mountain Facility, Wrightwood, CA, USA.
leblanc@tmf.jpl.nasa.gov, Tel: +1 760 249 1070, Fax: +1 760 249 5392

Alain Hauchecorne, and Philippe Keckhut
Service d'Aéronomie du CNRS, BP 3, 91371 Verrières-le-Buisson, France

1. Introduction

The middle atmosphere (20 to 90 km altitude) has received increasing interest from the scientific community during the last decades, especially since such problems as polar ozone depletion and climatic change have become so important. Temperature profiles have been obtained in this region using a variety of satellite-, rocket-, and balloon-borne instruments as well as some ground-based systems. One of the more promising of these instruments, especially for long-term high resolution measurements, is the lidar. Measurements of laser radiation Rayleigh backscattered [*Elterman*, 1951], or Raman scattered [*Moskowitz*, 1988], by atmospheric air molecules can be used to determine the relative air density profile and subsequently the temperature profile if it is assumed that the atmosphere is in hydrostatic equilibrium and follows the ideal gas law [*Hauchecorne and Chanin*, 1980]. The high vertical and spatial resolution make the lidar a well adapted instrument for the study of many middle atmospheric processes and phenomena as well as for the evaluation and validation of temperature measurements from satellites, such as the Upper Atmosphere Research Satellite (UARS). In the Network for Detection of Stratospheric Change (NDSC) [*Kurylo and Solomon*, 1990] lidar is the core instrument for measuring middle atmosphere temperature profiles. Using the best lidar analysis algorithm possible is therefore of crucial importance.

In this work, the JPL and CNRS/SA lidar analysis softwares were evaluated. The results of this evaluation allowed the programs to be corrected and optimized and new production software versions were produced. First, a brief description of the lidar technique and the method used to simulate lidar raw-data profiles from a given temperature profile is presented. Evaluation and optimization of the JPL and CNRS/SA algorithms are then discussed.

2. Determination of the atmospheric temperature profile from lidar measurements.

Laser radiation transmitted into the atmosphere is backscattered by the air molecules and collected by the lidar telescope. The number of photons received from a scattering layer δz, at a mean altitude z, is proportional to the number of photons emitted in the laser pulse and to the number of molecules or air density. Mie scattering by aerosols is typically only important below 25-30 km and can be neglected for the air density derivation above 30 km. However, following volcanic eruptions particular care is required to ensure that the density derivation is not corrupted by aerosol scattering. Then, the temperature is derived from the air density assuming hydrostatic equilibrium and the ideal gas law [*Hauchecorne and Chanin*, 1980].

3. Simulation of lidar raw-data.

Starting with known, user-defined temperature profiles the corresponding pressure and density profiles can be deduced and, in turn, theoretical or simulated raw-data profiles can be calculated using the known or measured characteristics of any specific lidar instrument. Simulated raw-data profiles are generated and then analyzed using the standard analysis algorithms as though they were measured profiles. The 'retrieved' temperature profiles are compared to the 'original' simulated ones. In this section, the simulation process is briefly described. Comparisons between retrieved and the original profiles will be presented in the next sections.

The first step in the data simulation procedure is the creation of the initial temperature profile. The CIRA-86 model was chosen as the climatological reference and as the starting point for the generation of test profiles. This model includes the zonal and monthly mean temperature between 0 and 100 km. The January-mean temperature profile at 44°N, 6°E was chosen as the basic reference profile. Various disturbances to this profile were introduced to simulate non-climatological profiles for the case studies described below.

The second step is to create the pressure-density profile associated with the generated temperature profile. A 2.7 hPa reference pressure at 40 km has been used to compute these profiles using the hydrostatic equilibrium and ideal gas law. The simulated interdependent temperature-pressure-density profile is then used to compute the theoretical number of photons that would be received by a given lidar instrument taking into account the known parameters of that

instrument. This is the main part of the simulation process.

1) The Rayleigh lidar equation is first evaluated, considering only the atmospheric backscattering and the constant terms relevant to the emitting system.

2) The Rayleigh extinction and ozone absorption corrections are then applied to the signal for the round-trip of the light between the instrument and the altitude of measurement. It is assumed here that no aerosols contribute to the signal extinction or backscattering, allowing comparisons of Rayleigh temperatures well below 30 km.

3) The signal is then corrected by the solid angle formed between the altitude of measurement and the telescope surface.

4) Then a noise from the sky background light must be added to the signal. When several independent channels are used, the sky background noise should be normalized by the fov of the telescopes when different.

5) The signal and sky background light are then transmitted between the receiving and counting systems. An efficiency coefficient has to be introduced to account for the optical transmission between the telescope surface and the photomultiplier detectors, and for the quantum efficiency of the counting system.

6) The photomultiplier and the counting system then translate the photons received into electronic pulses which are counted by the MCS. Due to the high dynamic range of the signal, the system can be either saturated if too many photons arrive in a short period or under-saturated if the magnitude of the electronic pulse caused by a low signal is too small to be retained [see for example, *Donovan et al.*, 1993]. The number of photons counted is therefore different from the true number of photons received. The correction applied is function of the maximum counting rate of the electronics and level of discrimination of the electronic pulses.

7) Finally, an instrumental noise has to be added. This so called signal-induced-noise is a reaction of the photomultipliers to the very strong signal received from the lower altitudes which results in a time dependent enhancement of the background counts.

The number of photons finally obtained is assumed to be the raw-data, as if it were really measured by the instrument. The output data must present signal levels similar to those obtained with real measurements since the analysis algorithms typically use these levels in various steps of the temperature derivation. To ensure that the results were not dependent on the simulations themselves, the latter were performed using characteristics typical of several different existing lidar systems. The simulated data are analyzed and the temperature results are compared to the original simulated temperature profiles.

The simulation of vibrational Raman lidar temperature measurements was also performed. The methods and equations used are similar to the Rayleigh simulation, except for few points (nitrogen density instead of air density, wavelengths and cross sections). Only the results from the Rayleigh simulations will be shown, since the results for the Raman case are strictly similar.

4. Evaluation of the JPL and CNRS/SA temperature lidar algorithms.

The simulation procedure described above was used to evaluate the temperature retrieval algorithms of the JPL and CNRS/SA lidar systems, and to diagnose inaccuracies or identify limitations in these analysis methods. Simulations were performed taking into account the actual characteristics of three different lidar systems: the Table Mountain Facility (TMF) and Mauna Loa Observatory (MLO) lidars of JPL, and the Observatoire de Haute-Provence (OHP) Rayleigh lidar system of CNRS/SA, France. Because the same analysis software is used for both TMF and MLO lidar systems, only MLO results will be shown, together with the OHP results.

As a starting point, a standard CIRA [*Fleming et al.*, 1990] temperature profile was used in the raw-data simulation. Since the lidar algorithms necessarily use model information in at least one part of the analysis, a simulated profile taken from a climatological model allows the study of analysis errors independent of the model errors. Raw data profiles corresponding to the CIRA-86 temperature profile at 44°N, 6°E in January were simulated and retrieved. Realistic experimental noise was included in the raw-data profiles to simulate a real data acquisition. The retrieved and original temperature profiles were compared. Both retrieved profiles remained close to the original, at least below 70 km (not shown). The MLO profile was systematically cut-off at 80 km, while the OHP profile was cut-off at a given signal to noise ratio. Some significant differences between the original and retrieved profiles appeared below 40 km for both the JPL and CNRS/SA profiles. These departures were much greater than the one sigma standard deviation, especially for the JPL profile below 25 km and were indicating that there were some problems with these versions of the algorithms.

To help identify the source(s) of the errors leading to such departures the same profile was simulated but without instrumental noise. Figures 1(a) and (b) show the difference between the retrieved and original simulated temperature profiles. At this point, the shape of the departures is clear, and the departures are apparently of different origin for OHP and MLO.

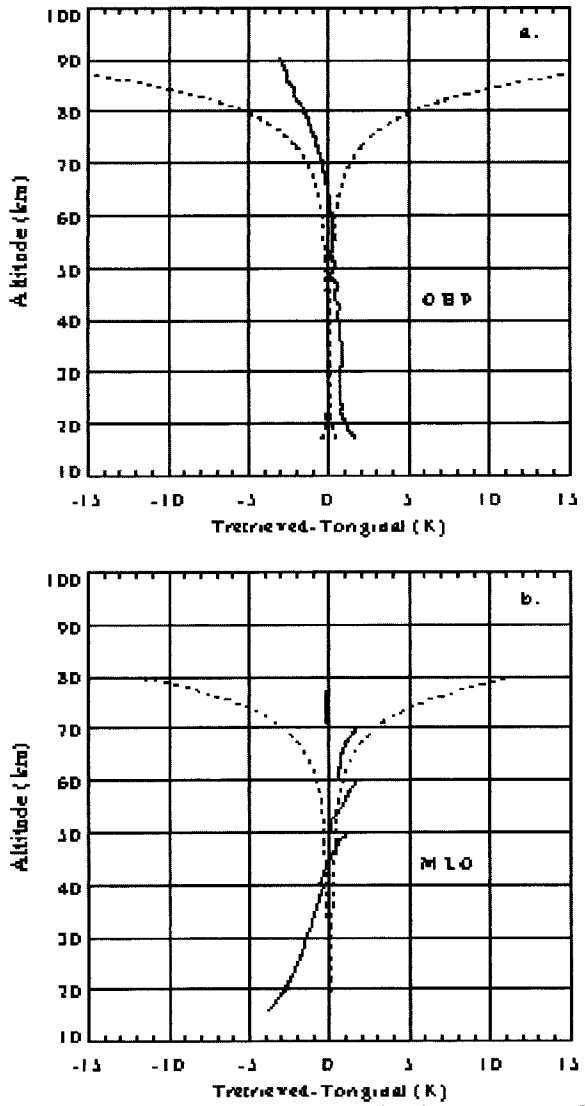

Figure 1: Deviation between the simulated (CIRA-86) profile and the OHP (a) and MLO (b) retrieved profiles. The dotted lines indicate the temperature error at one standard deviation

Large steps are observed every ten kilometers on the MLO which were not clear with the profiles containing instrumental noise. These steps were easily identified as being related to the smoothing part of the algorithm since they occur at the altitudes, every ten kilometers above 40 km, where the vertical smoothing range was increased. Review of the JPL algorithm revealed that a linear smoothing function was applied to the density signal which is actually an exponential function, decreasing with height. This source of inaccuracy was removed by applying the same smoothing method to the logarithm of the density which can be considered as a nearly linear function of altitude. Repeating the analysis with the corrected smoothing routine completely removes the steps (not shown here).

Several other departures were identified and corrected using the simulated data. Some of the errors identified have been summarized below:

- An error of few hundred meters in the site altitude assignment produces a maximum error of 5 K at 15 km, 2 K at 30 km, decreasing to near-zero as the altitude increases to 80 km.
- An error of a factor 2 in ozone vertical distribution causes a temperature error reaching more than 1 K at 20 km.
- An inaccurate background extraction (especially in the presence of non-linear signal induced noise) can lead to some errors reaching 5 K in the 10 upper kilometers of the profile.

5. Optimization of the JPL and CNRS/SA temperature lidar algorithms.

The simulation was then used to optimize the temperature retrievals of the JPL and CNRS/SA lidar systems. In this work, we will focus on a specific subject: The effect of introducing *a priori* information into the instrumental data, and the effect of smoothing. For lidar temperature retrievals, *a priori* information is necessary at two different steps in the data processing:

1) when normalizing the signal (relative density) to an *a priori* density taken from a CIRA-like climatological model or from a NCEP analysis.

2) when starting the downward integration of the temperature profile from the top.

Figure 2 illustrates, using the MLO retrieval, the effect of the temperature initialization at the top of the profile. The lidar temperature retrievals always need such an initialization which can be made by taking an *a priori* temperature and density or pressure at the top. The temperature profile is then integrated downward. In the case of Figure 2, the simulated profile is 15 K warmer than the CIRA profile at all altitudes. Therefore, when initializing at 90 km to the CIRA temperature, T_{TOP}, a -15 K departure is observed. Then, the error quickly decreases as we integrate downward because of the quasi-exponential growth of the density. Starting with a 15 K error at 90 km, it drops to 4 K at 80 km and 1 K at 70 km and becomes negligible below this. This error cannot be removed and can be a significant limitation of the lidar temperature analysis, especially near the mesopause which is a region with large temperature variability. However, Figure 2 illustrates the worst condition of using the *a priori* information since real temperature profiles are never 15 K hotter than the climatology throughout the entire profile (15-90 km). Even if deviations of 25-30 K occur at mesospheric heights, small vertical scale wave structures allow the real temperature to reach climatological values in several kilometers, making the

convergence from the outlying *a priori* values to the real values much faster.

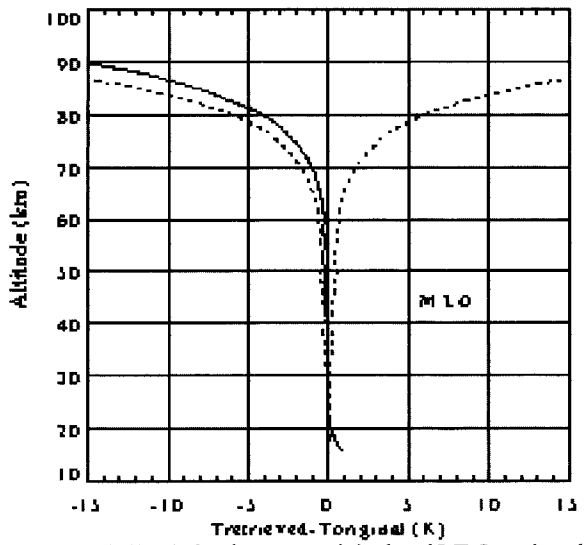

Figure 2: Deviation between original and MLO retrieved profiles for a simulated profile 15 K warmer than the standard CIRA profile.

6. Conclusion.

The use of simulation has been shown to be useful for testing the lidar analysis algorithms. Using known temperature-pressure-density profiles some typical raw-data profiles were simulated and then analyzed by different lidar softwares as if they had been obtained by real measurements. The retrieved temperature profiles were then compared to the simulated original profiles. By using different analysis methods, or by purposely introducing inaccuracies, the effects on the error related to different parts of the lidar analysis could be determined. Different error sources have been identified and quantified.

When the simulated profile is far from a climatological profile the most dramatic departures are located in the first 10 kilometers from the top due to the necessary initialization by model data (20 K departure of temperature is frequently observed). Also, the accuracy of the smoothing method and background subtraction are of crucial importance. A secondary effect is the inaccurate normalization of density, used in the extinction correction at UV wavelengths, leading to departures up to 3 K at the very bottom for UV wavelengths. Finally, range correction errors or altitude shifts can lead also to significant departures in the lower part of the profiles.

After these errors have been corrected the difference between retrieved and original profiles remained very small (< 0.5 K, not shown here), illustrating the usefulness of such approach. Other useful tests, concerning notably noise and saturation correction effects, can be investigated in the future simulations. The simulations presented in this work demonstrate the capability to evaluate lidar temperature analysis programs and to diagnose typical problems. Application of this technique to evaluate the different temperature analysis programs used by most of the lidar groups within the NDSC is planned.

Acknowledgments

The work described in this paper was carried out at the Jet Propulsion Laboratory, California Institute of Technology, under an agreement with the National Aeronautics and Space Administration.

References

Donovan, D. P., J. A. Whiteway, and A. I. Carswell, Correction for non-linear photon-counting effects in lidar systems, *Appl. Opt.*, *32*, 6742-6753, 1993.

Elterman, L. B., The measurement of stratospheric density distribution with the searchlight technique, *J. Geophys Res.*, *56*, 509-520, 1951.

Fleming, E. L., S. Chandra, J. J. Barnett, and M. Corney, COSPAR International Reference Atmosphere, Chapter 2: Zonal Mean Temperature, Pressure, Zonal Wind, and Geopotential Height as a Function of Latitude, *Adv. Space Res.*, *10*, 11-59, 1990.

Hauchecorne, A., and M. L. Chanin, Density and Temperature Profiles obtained by lidar between 35 and 70 km, *Geophys. Res. Lett.*, *8*, 565-568, 1980.

Kurylo M. J., and S. Solomon, Network for the Detection of Stratospheric Change: a status and implementation report, *NASA. Upper Atmosphere Research Program and NOAA Climate and Global Change Program*, NASA, Washington D.C., 1990.

Moskowitz, W. P., G. Davidson, D. Sipler, C. R. Philbrick, and P. Dao, Raman augmentation for Rayleigh lidar, 14th ILRC, Conference Abstracts, 284-286, 1988.